



Universidad Autónoma  
de Madrid

**Biblos-e Archivo**  
Repositorio Institucional UAM

**Repositorio Institucional de la Universidad Autónoma de Madrid**

<https://repositorio.uam.es>

Esta es la **versión de autor** del artículo publicado en:  
This is an **author produced version** of a paper published in:

Nanoscale Horizons 6.9 (2021): 744-750

**DOI:** <https://doi.org/10.1039/d1nh00184a>

**Copyright:** © 2021 The Royal Society of Chemistry

El acceso a la versión del editor puede requerir la suscripción del recurso  
Access to the published version may require subscription

# Efficient photogeneration of nonacene on nanostructured graphene

Cosme G. Ayani<sup>1,2,\*</sup>, Michele Pisarra<sup>2,3,\*</sup>, José I. Urgel<sup>2,4</sup>, Juan Jesús Navarro<sup>1,2,¶</sup>, Cristina Díaz<sup>3,6,†</sup>, Hironobu Hayashi<sup>5</sup>, Hiroko Yamada<sup>5</sup>, Fabian Calleja<sup>2</sup>, Rodolfo Miranda<sup>1,2,6</sup>, Roman Fasel<sup>4,7</sup>, Fernando Martín<sup>2,3,6,‡</sup>, Amadeo L. Vázquez de Parga<sup>1,2,6,‡</sup>

<sup>1</sup>Dep Física de la Materia Condensada, Universidad Autónoma de Madrid, Cantoblanco 28049, Madrid, Spain

<sup>2</sup>IMDEA-Nanociencia, Calle Faraday 9, Cantoblanco 28049, Madrid, Spain

<sup>3</sup>Dep. Química Módulo 13, Universidad Autónoma de Madrid, Cantoblanco, 28049 Madrid, Spain.

<sup>4</sup>Empa, Swiss Federal Laboratories for Material Science and Technology, 8600 Dübendorf, Switzerland.

<sup>5</sup>Graduate School of Science and Technology, Nara Institute of Science and Technology (NAIST), 8916-5 Takayama-cho, Ikoma 630-0192, Japan.

<sup>6</sup>Condensed Matter Physics Center (IFIMAC), Cantoblanco, 28049 Madrid, Spain.

<sup>7</sup>Department of Chemistry and Biochemistry, University of Bern, Freiestrasse 3, 3012 Bern, Switzerland.

<sup>†</sup>Present address: Departamento de Química Física, Facultad de C.C. Químicas, Universidad Complutense de Madrid, 28040 Madrid, Spain,

<sup>¶</sup>Present address: Department of Interface Science, Fritz-Haber Institute of the Max-Planck Society, 14195 Berlin, Germany

\* Authors contribute equally to this work

‡ Corresponding authors

## Abstract

The on-surface photogeneration of nonacene from  $\alpha$ -bisdiketone precursors deposited on nanostructured epitaxial graphene grown on Ru(0001) has been studied by means of low temperature scanning tunneling microscopy and spectroscopy. The presence of an unoccupied surface state, spatially localized in the regions where the precursors are adsorbed, and energetically accessible in the region of the electromagnetic spectrum where  $n\text{-}\pi^*$  transitions take place, allows for a 100% conversion of the precursors into nonacenes. With the help of state-of-the-art theoretical calculations, we show that such a high yield is due to the effective population of the surface state by the incoming light and the ensuing electron transfer to the unoccupied states of the precursors through an inelastic scattering mechanism. Our findings are the experimental confirmation that surface states can play a prominent role in the surface photochemistry of complex

molecular systems, in accordance with early theoretical predictions made on small molecules.

## INTRODUCTION

Surface photochemistry is a very active field of research due to its great potential in photocatalysis. It also has an intrinsic scientific interest, since it addresses fundamental aspects of the mechanism of energy transfer from the incident light to the molecules deposited on a substrate. In general, photochemical reactions are initiated by the absorption of photons, which is followed by different relaxation mechanisms that lead to the different products [1,2]. In surface photochemistry, the light can be directly absorbed by the adsorbate ("direct" mechanism) or the substrate ("indirect" or "substrate mediated" mechanism). For visible light, both processes imply electronic excitations of, respectively, the adsorbate or the substrate.

In the indirect mechanism, the photoelectrons carry the absorbed energy through the substrate and induce chemical reactions at the surface after localization on the adsorbate or the adsorbate-substrate complex. It is generally accepted that only those photoelectrons with energies that are resonant with adsorbate states (electron affinity levels) or adsorbate-substrate bonds can induce photochemistry. This condition is easily met for most metallic substrates, as the photoelectron energy distribution between the Fermi and the vacuum levels is usually broad and rather smooth, so there are always electrons with the appropriate energy to resonantly interact with the adsorbate. However, electron transfer from the surface to the adsorbate could be much more efficient when the photoelectron energy distribution builds up at the specific energies at which the adsorbate can host additional electrons [3,4].

The idea that surface localized photoelectrons can couple with molecular electronic states of the adsorbate first appeared in a theoretical study by Rous [5]. This work showed that the presence of substrate image states with an energy coincident with that of the  $N_2$  affinity levels increases the yield of the photochemical process by an order of magnitude. A similar enhancement of photochemical reactivity by surface states has been reported for other diatomic and triatomic molecules [6,7], but there is no evidence that this should also be the case for large molecular systems, as those used, e.g., in organic synthesis at surfaces, due to the more delocalized nature of the molecule's affinity levels.

In this respect, a particularly interesting area of research is the synthesis of large acenes on surfaces. Acenes, a family of polycyclic aromatic hydrocarbons consisting of linearly fused benzene rings, exhibit intriguing optical and electronic properties associated with their  $\pi$ -bond topology. One of the most appealing aspects in this regard is their extraordinarily narrow HOMO-LUMO gap, which makes them promising candidates as novel semiconducting materials [8-11]. Acenes can also be viewed as the narrowest members in the family of zig-zag graphene nanoribbons, which are predicted to host spin-polarized edge states

[12,13] and are postulated to be an important component in carbon-based spintronic devices. There is, however, a serious drawback to this ideal scenario: acenes longer than pentacene have low solubility and are highly reactive, which has prevented their synthesis and characterization in solution, with dimerization and photooxidation by molecular oxygen as typical degradation pathways [14-16]. Several strategies have been designed to overcome these problems, most of them relying on the insertion of the longer acenes in matrices of different materials that support and isolate them from the environment [17-19] or the functionalization with protecting groups [20-22]. But the main problem of these approaches is that they can modify the properties of the acenes and make their practical application difficult.

Very recently, several strategies for the on-surface generation of large acenes have been introduced [23-29]. Of particular interest is the visible-light induced photodecarbonylation of  $\alpha$ -bisdiketone precursors on Au(111) in Ultra-High Vacuum (UHV) [30]. In that work, 80% of the precursors were converted into nonacenes and heptacenes after 3 hours irradiation by 470 nm light with a photon flux at the sample of  $2.5 \times 10^{18} \text{ cm}^{-2} \text{ s}^{-1}$ . Now, Au(111) does not have surface states that actively participate in the acene formation, so the question that immediately arises is, would it be possible to reach even higher light-conversion yields for long-acene formation if substrates containing resonant surface states were used instead?

In this work, we have investigated the visible-light induced photodecarbonylation of  $\alpha$ -bisdiketone precursors on graphene epitaxially grown on Ru(0001) (hereafter called for short gr/Ru). The chosen substrate has unique electronic properties that makes it ideal to answer the posed question, since gr/Ru has an unoccupied electronic state at +2.85 eV above the Fermi level, which originates from the mixture of a Ru(0001) surface resonance and a graphene image state [31,32] and coincides in energy with the  $n-\pi^*$  transition of the diketone group [30]. We have found that when the original  $\alpha$ -bisdiketone precursors are deposited on gr/Ru and exposed to the same flux of visible light with the same wavelength of 470 nm for only 90 minutes a 100% yield is obtained, i.e. no precursors are observed on the surface. This represents a gain in light-conversion yield of more than a factor of two with respect to the Au(111) substrate, thus showing that the presence of resonant surface states is indeed a desirable feature to facilitate photochemical reactions of large organic molecules on solid substrates. The combination of low-temperature scanning tunneling microscopy (LT-STM) and spectroscopy (LT-STs) measurements and state-of-the-art density functional theory (DFT) calculations allows us to conclude that the higher yield observed for gr/Ru is due to (i) an efficient substrate light-adsorption due to the “d” bands of Ru, and (ii) an enhancement of the indirect mechanism by which photoelectrons mainly populate previously empty surface states in the low areas of the gr/Ru

moiré before they move over the unoccupied states of the precursors located there via an inelastic scattering process.

## RESULTS AND DISCUSSION

The difference in lattice parameter between graphene and Ru(0001) leads to a highly corrugated moiré pattern with a  $(12 \times 12)$  surface periodicity [33,34]. Consequently, the graphene carbon atoms are electronically inequivalent, which manifests in the X-ray C 1s photoelectron spectrum as two distinct C peaks [35]. Figure 1a shows an STM image with atomic resolution of the surface of a gr/Ru sample. The image shows two periodicities: the shortest one corresponds to the graphene atomic lattice, while the largest one, with a period of almost 3 nm, corresponds to the moiré unit cell  $(12 \times 12)$  (white rhombus). The bright protrusions in the image correspond to the areas where all carbon atoms are located above threefold hollow sites of the Ru surface. These are called Atop areas and are characterized by a weak van der Waals interaction between graphene and the substrate. Conversely, in the low areas (darker regions in Fig. 1) three C atoms are placed on top of the Ru surface atoms providing a strong covalent interaction with the substrate, whereas the remaining three C atoms are placed above threefold hollow sites. Within the low areas of the moiré pattern it is possible to distinguish two different zones according to the stacking of the carbon atoms located in threefold hollow sites with respect to the second Ru layer, denoted accordingly FCC-Top (blue circle) and HCP-Top (green circle). The presence of the moiré pattern locally modifies the electronic structure of the graphene overlayer [34,36].

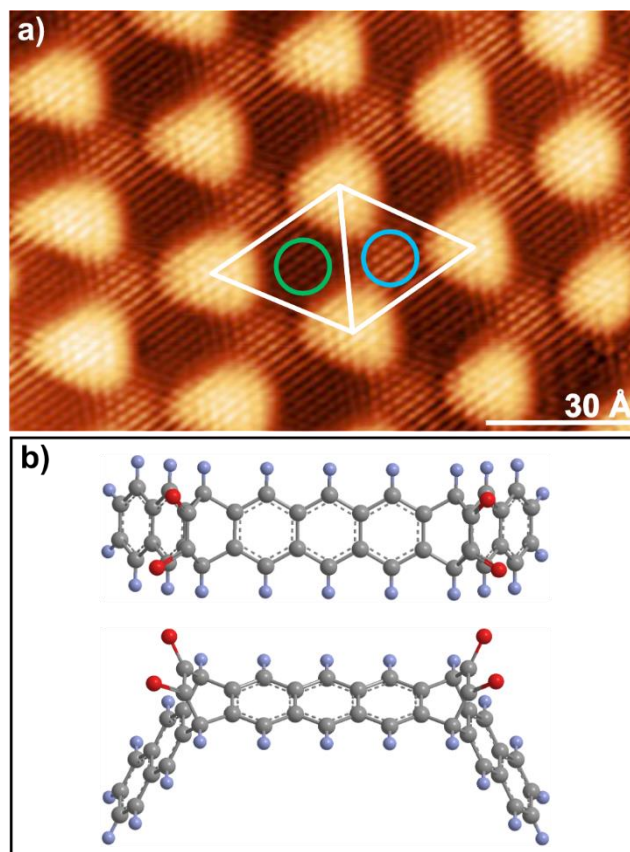


**Figure 1:** (a) Topographic STM image (13 nm x 8 nm),  $V_b = -5\text{mV}$ ,  $I_t = 100\text{pA}$  of gr/Ru(0001) surface containing several moiré unit cells (white rhombus). The green and blue circles indicate the so-called FCC-Top and HCP-Top areas of the moiré unit cell, respectively. The names indicate the registry with the ruthenium second layer of the three carbon atoms located at threefold hollow sites on the low areas of the moiré [34]. (b) Top and perspective views of the structure of the  $\alpha$ -bisdiketone nonacene precursors. Carbon and hydrogen atoms are represented in grey and blue, respectively, while the oxygens of each ketone group are represented in red.

A submonolayer coverage of  $\alpha$ -bisdiketone nonacene precursors, Figure 1b, was sublimated under dark conditions on a gr/Ru substrate held at room temperature. The inset in Figure 2a shows a constant-current STM image of an isolated precursor, exhibiting a rod-like appearance with two bright protrusions of similar apparent height, which we assign to the bridged  $\alpha$ -diketone groups pointing upwards. At higher coverages, the intact  $\alpha$ -bisdiketone nonacene precursors cover preferentially the low areas of the moiré pattern before populating the upper parts, as shown in Figure 2a. After deposition of the nonacene precursors, the sample was kept at room temperature and exposed to visible light ( $\lambda = 470\text{ nm}$ ,  $\Phi_{\text{photon}} = 2.5 \times 10^{18}\text{ cm}^{-2}\text{ s}^{-1}$ ) for 90 minutes. Upon irradiation, the photodecarbonylation of  $\alpha$ -bisdiketone nonacene precursors is achieved which gives rise to the formation of nonacenes. After light exposure the surface is covered with rod-like structures that are randomly distributed over the low areas of the moiré pattern of gr/Ru(0001) and are isolated from each other. Figure 2b shows an STM image of one of these rod-like structures that is uniform in apparent height. Our DFT calculations (see Materials and Methods) confirm that



nonacenes are physisorbed on the low areas of the gr/Ru(0001) moiré pattern (see Figure 2c). The DFT simulated STM image (right panel in Figure 2b) reproduces the intramolecular resolution in the experimental STM image (left panel in Figure 2b) and resembles the expected intramolecular resolution of the Lowest Unoccupied Molecular Orbital (LUMO) for a gas phase nonacene (see the SI). This indicates that the molecule is electronically decoupled from the substrate.

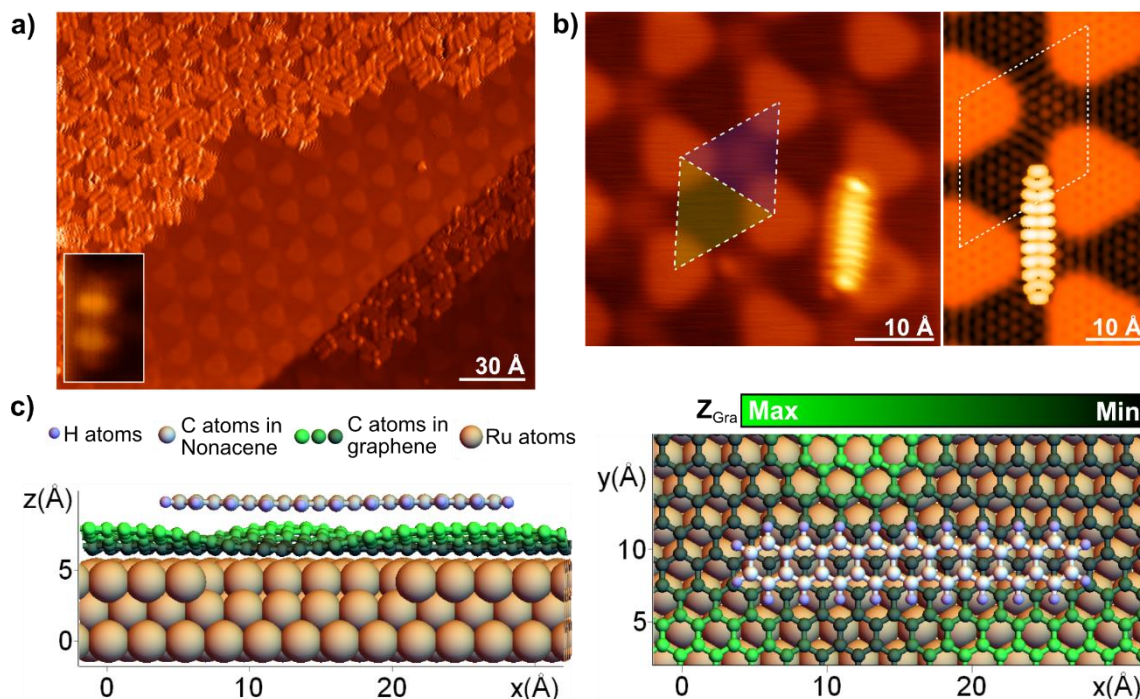


**Figure 2:** (a) STM topography ( $V_b = 1.5$  V,  $I_t = 50$  pA) image of  $\alpha$ -bisdiketone nonacene precursors on gr/Ru(0001) after room temperature deposition, recorded at 4.6K. The  $\alpha$ -bisdiketone nonacene precursors self-assemble by avoiding the ripples of the moiré pattern. Inset shows a topographic image of a single  $\alpha$ -bisdiketone nonacene precursor. The two bright protrusions are assigned to the  $\alpha$ -diketone groups pointing upwards [30]. (b) Left panel: STM image ( $V_b = 1.7$  V,  $I_t = 100$  pA) of a nonacene molecule adsorbed on the gr/Ru(0001) surface after being exposed to visible light ( $\lambda = 470$  nm) for 90 minutes. The right panel shows the simulated STM image. (c) DFT calculated geometry showing the most stable physisorbed configuration of a nonacene molecule on gr/Ru(0001). The left panel shows the lateral view and the right panel the top view. Color coding as indicated in the figure legend.

In order to determine the yield of the photogeneration process, we acquired STM images from different areas of the sample after exposure to light. In all the measured images, only nonacenes and no intact precursors were found (see section II in the SI for more details). From these data, we can conclude that a 100% conversion yield was achieved after 90 minutes of exposure to 470 nm light. In Table 1, we compare our results with those previously reported on Au(111) [30]. As can be seen, the on-surface photogeneration of nonacenes is significantly more efficient on gr/Ru(0001) despite the fact that photon fluence and wavelength are the same as in reference [30], and the latter was carefully



chosen to match the  $n-\pi^*$  transition of the diketone group and the first optical interband transition of gold [37] in order to promote Au(111) electrons into unoccupied orbitals of the precursors via inelastic scattering processes [38, 39].

	Au(111)	Gr/Ru(0001)
Light wavelength	470 nm	470 nm
Illumination time	3 hours	1.5 hours
Conversion yield	80%	100%

**Table 1:** Conversion yields for the photogeneration of nonacenes on Au(111) [30] and gr/Ru(0001) (this work). In both cases the conversion yield was obtained by evaluating STM images after light exposition on different locations of the sample.

The crucial factor for the high yield in the conversion is the presence of unoccupied surface states at the gr/Ru(0001) surface, which can host the hot electrons generated by the light adsorption process and facilitate their coupling with the molecular states. The presence of the graphene overlayer induces new states in the projected band gaps of Ru(0001), the so-called image states [40,41]. In free-standing graphene, due to the bidimensional nature of the material, image states appear on both sides of the graphene plane [42]. When the graphene layer approaches the Ru(0001) surface, the symmetry is broken thus leading to the disappearance of one set of image states. The energy position and the properties of the remaining states depend strongly on the distance between the graphene layer and the ruthenium surface [31]. According to state-of-the-art DFT calculations, this distance varies periodically along the moiré pattern, from around 3.4 Å on the ripples (Atop areas in Figure 1) to 2.2 Å on the lower areas of the moiré (HCP-Top and FCC-Top areas in Figure 1a) [41].

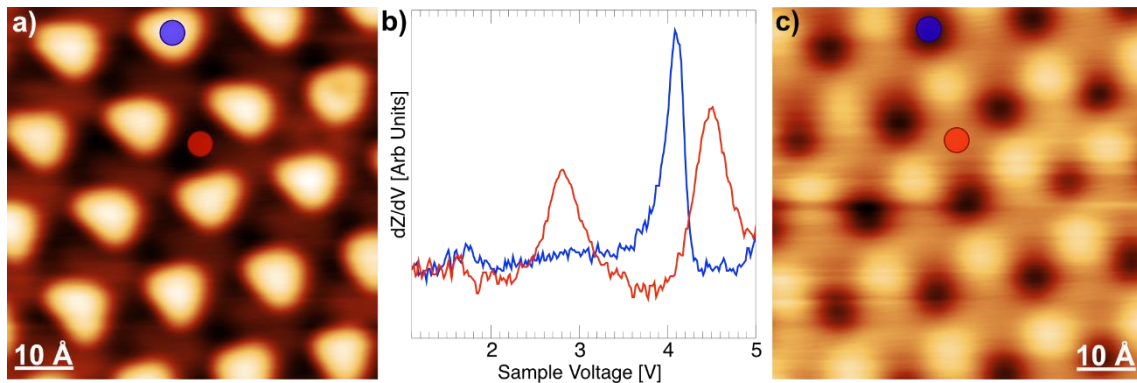


**Figure 3:** (a) STM topographic image ( $9 \times 9 \text{ nm}^2$ ,  $V_b = -0.5 \text{ V}$ ,  $I_t = 100 \text{ pA}$ ) measured at 4.6 K. (b)  $dZ/dV$  curves measured on the moiré superstructure reflecting the energy position of the corresponding field emission resonances. The blue curve was acquired on the ripples of the moiré (blue dot in panel a). The red curve was acquired on the low areas of the moiré (red dot in panel a). (c)  $dZ/dV$  map measured simultaneously with the image shown in panel a, showing the spatial distribution of the spectral feature appearing

in the red spectrum at +2.85 V in the low areas of the moiré. The coloured dots mark the same positions as in panel (a).

Figure 3a shows an STM image recorded on the gr/Ru sample; for the selected bias voltage, the ripples of the moiré superstructure appear as an ordered triangular array of protrusions. Figure 3b shows the  $dZ/dV$  curves measured on the ripples (blue curve) and the lower areas (red curve) of the moiré. In the curves measured on the ripples, where the distance between graphene and the metallic substrate is large, the first field emission resonance appears around +4.4 eV, close to the average work function measured on this surface [31]. The curves measured on the lower areas of the moiré, where the distance between graphene and ruthenium is small, exhibit two peaks in the energy range explored. The peak at + 2.85 eV is particularly interesting, because it is due to a surface localized one-electron state: it results from the interaction between the Ru(0001) surface resonance and the lowest image state of graphene [31,44,45]. In Figure 3c we show a  $dI/dV$  map measured at +2.85V, demonstrating that this surface state is uniformly distributed in the low areas of the moiré. Hence, the wave function of this surface state is localized precisely in the region where the nonacene precursors adsorb upon deposition at room temperature. This is a key factor for the on-surface photogeneration of nonacenes on gr/Ru(0001). The energy of this unoccupied surface state matches the energy of the  $n-\pi^*$  transition of the diketone group of the  $\alpha$ -bisdiketone nonacene precursor, and both the  $\alpha$ -bisdiketone nonacene precursors and the surface image state are spatially localized in the low areas of the moiré pattern (see Figure 2a and Figure 3c). Our results are thus the experimental realization of the scenario theoretically described by Rous [5], i.e. a system where the molecular resonance coincides in energy and space with an image state of the substrate.

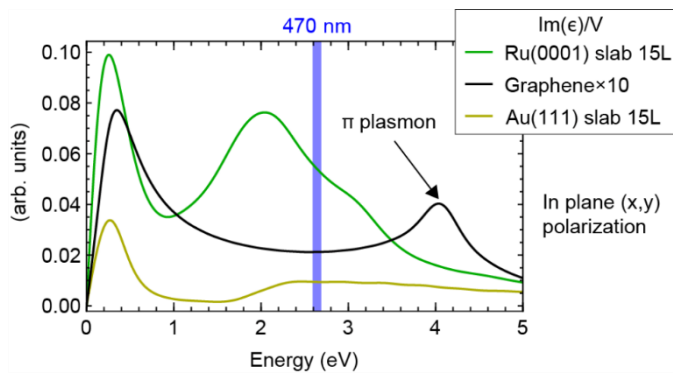


**Figure 4:** Imaginary part of the dielectric function,  $\epsilon_2(\omega) = \text{Im}[\epsilon(\omega)]$ , per unit volume, representing the optical properties of the three analyzed materials, as obtained in a Linear Response TD-DFT calculation. The graphene results are multiplied by 10 to visualize them on the same scale as those of Au and Ru. The vertical blue gridline marks the energy position of the light used in the experiments.

Finally, the high conversion efficiency observed in the experiment requires that the gr/Ru(0001) can efficiently absorb photons, thus ensuring the population of the surface states with hot electrons. In order to verify this, we performed Linear

Response TD-DFT calculations to retrieve the absorption properties of different materials and surfaces. In Figure 4 we present the imaginary part of the dielectric function per unit volume of a Ru(0001) surface, freestanding graphene and a Au(111) surface. The low-energy ends of the three spectra are dominated by the so-called Drude peak, which appears due to the conducting nature of the materials. The graphene spectrum, whose intensity is roughly one order of magnitude lower than those of the two metals, is also characterized by a peak at 4 eV, which is the ( $q \rightarrow 0$ ) one-body counterpart of the so called  $\pi$ -plasmon (see SI for more details), which is typical of graphene and graphitic materials [46-48]. The Au(111) spectrum presents a plateau starting at 2 eV, which corresponds to the onset of inter-band transitions from the  $d$  bands; we notice that the 470 nm wavelength falls within this plateau. Finally, the Ru(0001) absorption spectrum presents a high absolute value for the 470 nm wavelength and more features than Au(111) due to the presence of empty  $d$  bands just above the Fermi level (see also SI). The above analysis thus shows that the observed high photogeneration yield on gr/Ru(0001) results from the combination of (i) the high photon absorption on Ru(0001) and (ii) the appearance of a spatially localized surface state at the right energy due to the presence of the graphene adlayer.

In summary, we have shown that nonacene formation on gr/Ru(0001) can reach a 100% yield by exposing the corresponding  $\alpha$ -bisdiketone precursors to visible light of 470 nm. This represents a gain in light-conversion yield of more than a factor of two with respect to a Au(111) substrate under the same experimental conditions. This higher yield is the consequence of the efficient photon absorption by the ruthenium substrate, the appearance of an unoccupied surface state resonantly coupled to the  $\pi^*$  affinity levels of the precursors adsorbed on the low areas of the gr/Ru moiré pattern, and the spatial localization of this surface state in the same moiré regions. These results suggest that surface states can play a prominent role in the surface photochemistry of complex molecular systems by an appropriate selection of a substrate that fulfills the above criteria.

## Acknowledgements

Work partially supported by the Ministerio de Ciencia, Innovación y Universidades projects PGC2018-093291-B-I00, CTQ2017-83531-R, PID2019-105458RB-I00 and PID2019-106732GB-I00 and Comunidad de Madrid projects NMAT2D-CM P20128/NMT-4511 and NanoMagCost. IMDEA Nanoscience acknowledges support from the “Severo Ochoa” Programme for Centres of Excellence in R&D (MINECO, grant SEV-2016-0686). IFIMAC acknowledges support from the “María de Maeztu” Programme for Units of Excellence in R&D (MINECO, grant MDM-2014-0377). Empa acknowledges support by the Swiss National Science Foundation under Grant No. 200020-182015. We acknowledge the allocation of computer time by the Red Española de Supercomputación and the Centro de Computación Científica at the Universidad Autónoma de Madrid

(CCC-UAM). NAIST acknowledges support by CREST (JPMJCR15F1) and Grants-in-Aid for Scientific Research (JP20H02816).

## **MATERIALS AND METHODS**

### **Sample preparation**

The Ru(0001) crystal was Ar<sup>+</sup> sputtered, heated in oxygen and flash annealed in vacuum until a (1x1) LEED pattern and no traces of contaminants were observed. The graphene samples on Ruthenium were prepared keeping the Ru crystal at 1150 K in UHV and exposed to ethylene at pressures of  $2 \times 10^{-7}$  mbar for 3 min (48 L, 1 L =  $1.33 \times 10^{-6}$  mbar s). The temperature was held at 1150K for a further 2 min after removing the C<sub>2</sub>H<sub>4</sub> gas from the chamber. The synthesis of the molecular precursors is described in reference [30]. Molecular precursors were thermally deposited onto a clean gr/Ru(0001) surface held at room temperature. The deposition rate was  $0.4 \text{ \AA min}^{-1}$  for a sublimation temperature of 610 K. After precursor deposition, the sample was exposed to visible light (Blue (470 nm) LUXEON Rebel LED, mounted on a 40 mm round base with seven LEDs, 490 lm @ 700 mA). During the exposure to light, the sample was kept at room temperature. Subsequently, the sample was introduced in the STM and cooled down to 4.8 K or 1.2 K for inspection. The light source was located outside the STM chamber at approximately 20 cm from the sample and in front of the surface. The estimated photon flux at the sample is  $2.5 \times 10^{18} \text{ cm}^{-2} \text{ s}^{-1}$ .

### **STM experiments**

All experiments were performed in a UHV chamber with a base pressure of  $5 \times 10^{-11}$  mbar equipped with an LT-STM and facilities for tip and sample preparation. The clean W tips were prepared by Ar<sup>+</sup> sputtering (2.5 keV) in UHV for 45 min and then heated up by resistive heating. All the STM/STS data were measured with both tip and sample at 4.8 K or 1.2 K.

### **DFT and TD-DFT calculations**

DFT based calculations have been carried out using the PAW method [47] (400 eV PW cut-off), as implemented in the VASP package [49-52], using the PBE [53] exchange-correlation functional plus the Tkatchenko-Sheffler [54] correction, to take into account weak dispersion forces. The graphene ruthenium surface was modelled by a three-layer thick Ru slab oriented in the (0001) direction with a graphene layer adsorbed on one side. To simulate the adsorption of nonacene, we adopted a (22x11)Graphene/(20x10)Ru supercell to minimize the molecule-molecule interactions in the periodic replicas using at least a 20 Å vacuum region in the out of plane direction; notice that the (11x11)Graphene/(10x10)Ru supercell, is capable of reproducing all the physical properties of the graphene ruthenium moiré [43]. A full relaxation of the nonacene atoms and of the graphene atoms was carried out until the residual forces on the active atoms were less than

0.01 eV/ Å, limiting the Brillouin Zone integration to the  $\Gamma$  point. The simulated STM images were calculated by the Tersoff Hamann method [55]. The images are obtained calculating the isosurfaces of the electron density integrated in the energy window going from the Fermi level to the bias energy,  $E_b = eV_b$ , where  $V_b$  is the bias voltage and  $e = 1.6 \times 10^{-19}$  C is the elementary charge. The isovalue ( $I_{\text{sov}}$ ) in  $\text{\AA}^{-3}$  is obtained by the equation  $I_{\text{sov}} = 2 \times 10^{-4} \sqrt{I_t}$  in which the tunnelling current ( $I_t$ ) value is expressed in nA.

The Linear Response TD-DFT calculations were carried out using the PAW based implementation available within the VASP package [56]. The ruthenium and gold surfaces were modeled by 15 layer thick slabs (30 Å vacuum region) oriented in the (0001) and (111) directions, respectively, relaxing the coordinates of the outermost layers. The light absorption is calculated as the imaginary part of the dielectric function,  $\epsilon_2(\mathbf{q}, \omega)$ , normalized to the total volume, in the long wavelength limit ( $\mathbf{q} \rightarrow 0$ ), and neglecting local field effects. The TD-DFT runs were carried out using unshifted  $36 \times 36 \times 1$  k-point mesh ( $60 \times 60 \times 1$  for graphene). We enforced a very strict  $10^{-8}$  eV energy tolerance, to ensure precise convergence of the Kohn Sham wave functions, including in the calculation a total of 256, 180, and 60 bands, for the Ru(0001), Au(111), and graphene, respectively, sampling the energy region up to 20 eV above the Fermi level.

## BIBLIOGRAPHY

- [1] F.M. Zimmermann, W. Ho, Vibrational excitation dynamics in photodesorption, *Surf. Sci. Rep.* **1995**, 22, 127.
- [2] J.C. Tully, Chemical dynamics at metal surfaces, *Annu. Rev. Phys. Chem.* **2000**, 51, 153.
- [3] C. Frischkorn and M. Wolf, Femtochemistry at metal surfaces: Nonadiabatic reaction dynamics, *Chem. Rev.* **2006**, 106, 4207.
- [4] C.D. Lindstrom and X.-Y. Zhu, Photoinduced electron transfer at molecule-metal interfaces, *Chem Rev.*, **2006**, 106, 4281-4300.
- [5] P.J. Rous, Negative ion formation in adsorbed molecules: the role of surface states, *Phys. Rev. Lett.* **1995**, 74, 1835-1838.
- [6] K.B.K. Tang, P.J. Rous & R.E. Palmer, Energy lifetime of the  $\sigma$  resonance of oriented  $\text{O}_2$  physisorbed on Ag(110), *Phys. Rev. B*, **1995**, 52, 12395.
- [7] E.T. Jensen, Charge-transfer photodissociation of adsorbed molecules via electron image states, *J. Chem. Phys.* **2008**, 128, 044301.
- [8] J.E. Anthony, The larger acenes: versatile organic semiconductors. *Angew. Chem. Int. Ed.* **2008**, 47, 452–483.
- [9] J.E. Anthony, Functionalized acenes and heteroacenes for organic electronics. *Chem. Rev.* **2006**, 106, 5028–5048.
- [10] Z. Sun, Q. Ye, C. Chi, & J. Wu, Low band gap polycyclic hydrocarbons: from closed-shell near infrared dyes and semiconductors to open-shell radicals. *Chem. Soc. Rev.* **2012**, 41, 7857–7889.



- [11] M. Watanabe et al., The synthesis, crystal structure and charge transport properties of hexacene. *Nat. Chem.* **2012**, 4, 574–578.
- [12] M. Fujita, K. Wakabayashi, K. Nakada & K. Kusakabe, Peculiar localized state at zigzag graphite edge. *J. Phys. Soc. Jpn.* **1996**, 65, 1920–1923.
- [13] P. Ruffieux et al. On-surface synthesis of graphene nanoribbons with zigzag edge topology. *Nature* **2016**, 531, 489–492.
- [14] D. Biermann & W. Schmidt, Diels-Alder reactivity of polycyclic aromatic hydrocarbons. Acenes and benzologs. *J. Am. Chem. Soc.* **1980**, 102, 3163–3173.
- [15] A.R. Reddy, G. Fridman-Marueli & M. Bendikov, Kinetic and thermodynamic stability of acenes: theoretical study of nucleophilic and electrophilic addition. *J. Org. Chem.* **2007**, 72, 51–61.
- [16] P. von Schleyer, R., Manoharan, H Jiao, & F. Stahl, The acenes: is there a relationship between aromatic stabilization and reactivity? *Org. Lett.* **2001**, 3, 3643–3646.
- [17] R. Mondal, R.M. Adhikari, B.K. Shah, & D.C. Neckers, Revisiting the stability of hexacenes. *Org. Lett.* **2007**, 9, 2505–2508.
- [18] R. Mondal, B. Shah & D.C. Neckers, Photogeneration of heptacene in a polymer matrix. *J. Am. Chem. Soc.* **2006**, 128, 9612–9613.
- [19] C. Tønshoff & H.F. Bettinger, Photogeneration of octacene and nonacene. *Angew. Chem. Int. Ed.* **2010**, 49, 4125–4128.
- [20] R. Dorel & A.M. Echavarren, Strategies for the synthesis of higher acenes. *Eur. J. Org. Chem.* **2017**, 14–24.
- [21] H.F. Bettinger & C. Tønshoff, The longest acenes. *Chem. Rec.* **2015**, 15, 364–369.
- [22] M. Watanabe, et al. The synthesis, crystal structure and charge-transport properties of hexacene. *Nat. Chem.* **2021**, 4, 574–578.
- [23] J.I. Urgel et al., On-surface synthesis of heptacene organometallic complexes. *J. Am. Chem. Soc.* **2017**, 139, 11658–11661.
- [24] M. Zugermeier et al. On-surface synthesis of heptacene and its interaction with a metal surface, *Nanoscale* **2017**, 9, 12461.
- [25] R. Zuzak et al., Nonacene generated by on-surface dehydrogenation. *ACS Nano* **2017**, 11, 9321–9329.
- [26] L. Colazzo et al., On-surface synthesis of heptacene on Ag (001) from brominated and non-brominated tetrahydroheptacene precursors. *Chem. Comm.* **2018**, 54, 10260–10263.
- [27] R. Zuzak et al., Higher Acenes by On-Surface Dehydrogenation: From Heptacene to Undecacene. *Angew. Chem. Int. Ed.* **2018**, 57, 10500–10505.
- [28] J. Krüger et al., Decacene: On-Surface Generation. *Angew. Chem.* **2017**, 129, 12107–12110.
- [29] F. Eisenhut et al. Dodecacene generated on surface: reopening of the energy gap. *ACS Nano* **2019**, 14, 1011–1017.
- [30] J.I. Urgel et al., On-surface light-induced generation of higher acenes and elucidation of their open-shell character, *Nat. Comm.* **2019**, 10, 861.
- [31] B. Borca, S. Barja, M. Garnica, D. Sánchez-Portal, V.M. Silkin, E.V. Chulkov, C.F. Hermanns, J.J. Hinarejos, A.L. Vázquez de Parga, A. Arnau, P.M. Echenique, R.

Miranda, Potential Energy Landscape for Hot Electrons in Periodically Nanostructured Graphene, *Phys. Rev. Lett.* **2010**, 105, 036804.

[32] N. Ambrust, J. Gdde, P. Jakob, U. Hfer, Time resolved two photon photoemission of unoccupied electronic states of periodically rippled graphene on Ru(0001), *Phys. Rev. Lett.* **2012**, 108, 056801.

[33] S. Marchini, S. Gnther, J. Wintterlin, Scanning tunneling microscopy of graphene on Ru(0001). *Phys. Rev. B* **2007**, 76, 075429.

[34] A. L. Vzquez de Parga, F. Calleja, B. Borca, M. C. G. Passeggi Jr., J. J. Hinarejos, F. Guinea, R. Miranda, Periodically rippled graphene: Growth and spatially resolved electronic structure. *Phys. Rev. Lett.* **2008**, 100, 056807.

[35] A.B. Preobrajenski, M.L. Ng, S. Vinogradov & N. Martensson, Controlling Graphene corrugation on lattice-mismatched substrates, *Phys. Rev. B* **2008**, 78, 073401.

[36] B. Borca, S. Barja, M. Garnica, M. Minniti, A. Politano, J. M. Rodriguez-García, J. J. Hinarejos, D. Farías, A. L. Vzquez de Parga, R. Miranda, Electronic and geometric corrugation of periodically rippled, self-nanostructured graphene epitaxially grown on Ru(0001). *New J. Phys.* **2010**, 12, 093018.

[37] P.B. Johnson, R.W. Christy, Optical constants of the noble metals. *Phys. Rev. B* **1972**, 6, 4370 – 4379.

[38] C. Frischkorn and M. Wolf, Femtochemistry at metal surfaces: Nonadiabatic reaction dynamics, *Chem. Rev.* **2006**, 106, 4207.

[39] C.D. Lindstrom and X.-Y. Zhu, Photoinduced electron transfer at molecule-metal interfaces, *Chem. Rev.* **2006**, 106, 4281-4300.

[40] P.M. Echenique & J.B. Pendry, The existence and detection of Rydberg states at surfaces, *J. Phys. C* **1978**, 11, 2065.

[41] F.J. Himpsel, K. Christman, P. Heimann, D.E. Eastman & P.J. Feibelman, Adsorbate band dispersion for C on Ru(001), *Surf. Sci.* **1982**, 115, L159.

[42] V.M. Silkin, J. Zhao, F. Guinea, E.V. Chulkov, P.M. Echenique & H. Petek, Image potential states in graphene, *Phys. Rev. B* **2009**, 80, 121408R.

[43] D. Stradi. S. Barja, C. Daz, M. Garnica, B. Borca, J.J. Hinarejos, D. Snchez-Portal, M. Alcam, A. Arnau, A.L. Vzquez de Parga, R. Miranda, F. Martn, Role of the dispersion forces in the structure of graphene monolayers on Ru surfaces., *Phys. Rev. Lett.* **2011**, 106, 186102.

[44] N. Ambrust, J. Gdde, P. Jakob & U. Hfer, Time-resolved two-photon photoemission of unoccupied electronic states of periodically rippled graphene on Ru(0001), *Phys. Rev. Lett.* **2021**, 108, 056801.

[45] V. del Campo, J.D. Correa, J. Correa-Puerta, D. Kroeger, P. Hberle, Unoccupied electronic states of Ru(0002), *Surf. Sci.* **2016**, 653, 163.

[46] V. Despoja, D. Novko, K. Dekani, M. unji, and L. Marui, Two-dimensional and pi-plasmon spectra in pristine and doped graphene, *Phys. Rev. B* **2013**, 87, 075447.

[47] M. Pisarra, A. Sindona, M. Gravina, V. M. Silkin, and J. M. Pitarke, Dielectric screening and plasmon resonances in bilayer graphene, *Phys. Rev. B* **2016**, 93, 035440.

[48] C. Vacacela Gomez, M. Pisarra, M. Gravina, P. Riccardi, and A. Sindona, Plasmon properties and hybridization effects in silicene, *Phys. Rev. B* **2017**, 95, 085419.



- [49] P. E. Blochl, Projector Augmented-Wave Method. *Phys. Rev. B* **1994**, 50, 17953.
- [50] G. Kresse and D. Joubert, From ultrasoft pseudopotentials to the projector augmented-wave method. *Phys. Rev. B* **1999**, 59, 1758.
- [51] G. Kresse and J. Furthmuller, Efficiency of ab-initio total energy calculations for metals and semiconductors using a plane-wave basis set. *Computational Material Science* **1996**, 6, 15.
- [52] G. Kresse and J. Furthmuller, Efficient iterative schemes for ab initio total-energy calculations using a plane-wave basis set. *Phys. Rev. B* **1996**, 54, 11169.
- [53] J. P. Perdew, K. Burke and M. Ernzerhof, Generalized Gradient Approximation Made Simple. *Phys. Rev. Lett.* **1996**, 77, 3865.
- [54] A. Tkatchenko and M. Scheffler, Accurate Molecular Van Der Waals Interactions from Ground-State Electron Density and Free-Atom Reference Data, *Phys. Rev. Lett.* **2009**, 102, 073005.
- [55] J. Tersoff, D. R. Hamman, Theory and application for the scanning tunneling microscope. *Phys. Rev. Lett.* **1983**, 50, 1998–2001.
- [56] M. Gajdos, K. Hummer, G. Kresse, J. Furthmuller, and F. Bechstedt, Linear optical properties in the projector-augmented wave method. *Phys. Rev. B* **2006**, 73, 045112.